JOURNAL OF GEOPHYSICAL RESEARCH, VOL. 105, NO. A9, PAGES 20,957–20,971, SEPTEMBER 1, 2000

Electron temperature and de Hoffmann-Teller potential change across the Earth's bow shock: New results from ISEE 1

A. J. Hull[1] and J. D. Scudder

Department of Physics and Astronomy, University of Iowa, Iowa City

R. J. Fitzenreiter and K. W. Ogilvie

NASA Goddard Space Flight Center, Greenbelt, Maryland

J. A. Newbury and C. T. Russell

Institute of Geophysics and Planetary Physics, University of California, Los Angeles

Abstract. We present a survey of the trends between the electron temperature increase ΔT_e and the de Hoffmann-Teller frame (HTF) electrostatic potential jump $\Delta\Phi^{HT}$ and their correlation with other parameters that characterize the shock transition using a new ISEE 1 database of 129 Earth bow shock crossings. A fundamental understanding of the HTF potential is central to distinguishing the reversible and irreversible changes to electron temperature across collisionless shocks. The HTF potential is estimated using three different techniques: (1) integrating the steady state, electron fluid momentum equation across the shock layer using high time resolution plasma and field data from ISEE 1, (2) using the steady state, electron fluid energy equation, and (3) using an electron polytrope approximation. We find that $\Delta\Phi^{HT}$ and ΔT_e are strongly and positively correlated with $|\Delta(m_p U_n^2/2)|$, which is in good qualitative agreement with earlier experimental surveys [*Thomsen et al.*, 1987b; *Schwartz et al.*, 1988] that used bow shock model normals and used the flow in the spacecraft frame. There is a strong linear organization of the ΔT_e with $\Delta\Phi^{HT}$, which suggests an average effective electron polytropic index of $\langle\gamma_e\rangle \approx 2$. In addition, ΔT_e and $\Delta\Phi^{HT}$ are organized by β_e, although our results may be biased by our limited sampling of shock conditions. Comparisons indicate that the differentials in the HTF potential $\delta\Phi^{HT}$ are proportional to the differentials in the magnetic field intensity δB across the shock, with a proportionality constant κ that is a fixed constant for a given shock crossing.

1. Introduction

The cross-shock potential and its relation to electron temperature changes ΔT_e at collisionless, fast mode shocks have been subjects of interest for quite some time. The notion that the cross-shock potential may be important in changing the electron temperature across strong, fast mode shocks was introduced by *Feldman et al.* [1982]. *Feldman et al.* [1982, 1983b] reported observations of a field-aligned, downstream directed electron beam at the outer edge of a "flat-topped" background electron velocity distribution within the magnetic ramp of the Earth's quasi-perpendicular bow shock. Motivated by the apparent acceleration and relaxation of the electron beams, *Feldman et al.* [1982, 1983b] proposed a two-step process which consists of a downstream acceleration along the magnetic field followed by beam-driven plasma instabilities as the mechanism for causing ΔT_e across strong shocks (downstream-upstream field ratio $B_2/B_1 \rightarrow 4$). In contrast, *Feldman et al.* [1983a] demonstrated using perpendicular and parallel two-dimensional (2-D) measurements of the electron distribution that ΔT_e at weak shocks ($B_2/B_1 \rightarrow 1$) was consistent with the conservation of the electron magnetic moment.

The effect of the potential on the behavior of magnetized electrons across collisionless shocks was addressed

[1]Now at Space Science Laboratory, University of California, Berkeley.

Copyright 2000 by the American Geophysical Union.

Paper number 2000JA900049.
0148-0227/00/2000JA900049$09.00

in the theoretical study by *Goodrich and Scudder* [1984]. An important point raised by *Goodrich and Scudder* [1984] not appreciated in early studies was that although ΔT_e is frame independent, the electrostatic potential is not. With this in mind, *Goodrich and Scudder* [1984] demonstrated that the potential in the de Hoffmann-Teller frame (HTF) determines the electric field most relevant to understanding electron energetics and predicting ΔT_e across collisionless shocks. The HTF is that special shock rest frame in which the motional electric field vanishes ($\mathbf{E}_m^{HT} = -\mathbf{U}^{HT} \times \mathbf{B}/\mathbf{c} = 0$). As a result, the MHD center of mass velocity of the fluid flow, $\mathbf{U}^{HT}$, is field aligned on either side of the shock. Accordingly, the electric field in this frame only has a nonvanishing component along the shock normal within the shock layer with a sense to simultaneously (1) decelerate ions and (2) accelerate electrons as they cross the shock from the low- to the high-density side. In HTF the electrons only get energized by the cross-shock potential jump $\Delta\Phi^{HT}$. There is no exchange between the particles and the Poynting flux $\mathbf{S}$, because $\mathbf{S}$ is zero in this frame. Moreover, *Scudder* [1987] demonstrated theoretically and with a strong Earth bow shock observed by ISEE 1 that in HTF the electron bulk flow within the shock layer is approximately field aligned as long as pressure anisotropy, electron inertia, and resistive effects can be neglected.

The effect of the HTF electrostatic potential $\Phi^{HT}(x)$ on the shape of the electron distribution function was first successfully tested [*Scudder et al.*, 1986c] by employing Liouville's theorem to map $v_\perp = 0$ cuts of the upstream and downstream boundary electron distribution function to regions within the resolved layer of a supercritical, fast mode shock observed by ISEE 1. Contrasting the observed electron distribution function with the predictions of Vlasov theory in the smooth forces, *Scudder et al.* [1986c] showed that $\Phi^{HT}(x)$ is responsible for most of the broadening of the electron distribution, at least along the magnetic field, and possibly could explain the temperature increase and the observed electron distribution function signatures typically observed across supercritical, fast mode shocks. The wave-particle interactions are found to provide secondary irreversible, collective cooling.

In more recent studies [*Scudder*, 1995; *Hull et al.*, 1998] the Vlasov-Liouville (V-L) mapping technique was applied to model electron distribution functions to demonstrate that the steady state, macroscopic electric and magnetic fields acting on magnetized electrons can explain the electron velocity distribution signatures at all pitch angles and hence explain much of the electron heating morphology at both strong and weak shocks. As suggested by *Scudder* [1995], the V-L mapping procedure does recover [*Hull et al.*, 1998] the preferential perpendicular inflation signatures observed at weak shocks [*Feldman et al.*, 1983b], as well as the nearly isotropic inflation signatures observed at strong shocks [*Montgomery et al.*, 1970; *Scudder et al.*, 1973; *Feldman et al.*, 1983a; *Scudder et al.*, 1986a] without invoking wave-particle effects. Moreover, trends in the perpendicular and parallel electron temperature increase typically observed across strong and weak shocks are qualitatively recovered [*Hull et al.*, 1998] by the V-L model coupled with the Rankine-Hugoniot conservation laws and using a maximal trapping assumption [*Morse*, 1965; *Forslund and Shonk*, 1970; *Scudder et al.*, 1986c]. *Hull et al.* [1998] also used 3-D electron distribution function data observed at a very weak shock by Galileo to show that the V-L technique can recover the downstream electron distribution function at all pitch angles and therefore explains the observed ΔT_e.

Despite the progress made in understanding the role played by the dc forces on producing the signatures of the electron distribution functions and the impact these coherent forces have on changing electron temperature across fast mode shocks, very few studies [*Thomsen et al.*, 1987a; *Schwartz et al.*, 1988] have focused on the statistical properties of $\Delta\Phi^{HT}$ and its relation to ΔT_e and other characteristic shock fluid parameters. The statistical studies of *Thomsen et al.* [1987a] and *Schwartz et al.* [1988] used the electron polytrope expectation ($\Delta\Phi^{HT} \propto \Delta T_e$ [*Goodrich and Scudder*, 1984]) to estimate the HTF cross-shock potential. *Thomsen et al.* [1987a] showed that the ratio $\Delta\Phi^{NIF}/\Delta\Phi^{HT}$ (where $\Delta\Phi^{NIF}$ is the normal incidence frame cross-shock potential) is typically 2-6 and has a slight dependence on θ_{Bn1}. The range of $\Delta\Phi^{NIF}/\Delta\Phi^{HT}$ is consistent with previous empirical estimates [*Goodrich and Scudder*, 1984]. These results together with the observational evidence that the magnetic field rotates out of the coplanarity plane in a fast mode sense [*Thomsen et al.*, 1987a] and a slow mode sense [*Scudder*, 1995] empirically established the frame dependence of the cross-shock potential suggested by *Goodrich and Scudder* [1984]. A major result of the studies by *Thomsen et al.* [1987b] and *Schwartz et al.* [1988] was that ΔT_e (or $\Delta\Phi^{HT}$ computed via polytrope assumption) was found to be strongly correlated with the change in the flow energy $U_2^2 - U_1^2$ in the spacecraft frame. *Thomsen et al.* [1987b] and *Schwartz et al.* [1988] argued that the strong dependence of ΔT_e on $U_2^2 - U_1^2$ was consistent with a process initiated by the cross-shock electrostatic potential and that this first-order dependence on $U_2^2 - U_1^2$ should be normalized out. Thus *Schwartz et al.* [1988] demonstrated that $\Delta\Phi^{HT}$ normalized by the incident proton ram energy $m_p U_1^2$ decreased with increasing Mach number and did not seem to strongly depend on shock geometry θ_{Bn1}, total upstream plasma β_{tot1}, and upstream electron-ion temperature ratio T_{e1}/T_{p1}. However, the results of these studies which use the flow in the spacecraft frame can be inaccurate since the relevant flow is that along the shock normal in the shock stationary frame.

This work extends the statistical studies of *Thomsen et al.* [1987a] and *Schwartz et al.* [1988] by using a new ISEE 1 database of 129 Earth bow shock observations

corrected for the spacecraft floating potential and characterized by the best possible determination of the local shock geometry from asymptotic moment and magnetic field data under a Rankine-Hugoniot formalism. In the present study we determined statistically for the first time $\Delta\Phi^{\mathrm{HT}}$ using two model-free approaches and compared these determinations to the electron polytrope expectation assumed in earlier statistical studies [*Thomsen et al.*, 1987a; *Schwartz et al.*, 1988]. The empirically determined $\Delta\Phi^{\mathrm{HT}}$ is compared with ΔT_{e} and other parameters that characterize the macroscopic state of these shock observations such as the angle between the upstream magnetic field and shock normal θ_{Bn1}, the upstream electron $\beta_{\mathrm{e}1}$, and upstream electron HTF thermal Mach number $M_{\mathrm{HTF}} = U_{n1}/(V_{\mathrm{the}1}\cos\theta_{Bn1})$. Finally, we test the validity of the $\Delta\Phi^{\mathrm{HT}} = \kappa\Delta B$ assumption used in earlier theoretical studies of electron kinetics across fast mode shocks [e.g., *Scudder*, 1995; *Hull et al.*, 1998].

2. Instrumentation and Experimental Data Set

An extensive electron moment and magnetic field data set of 129 Earth bow shock events observed by ISEE 1 from 1977 to 1979 has been analyzed including separate Rankine-Hugoniot analysis of shock geometry and shock velocity (discussed below). The electron moment data used in this study are derived (after taking the instrument characteristics into account) from electron counting rates measured by the vector electron spectrometer (VES) on board ISEE 1 [*Ogilvie et al.*, 1978]. The full 3-D electron measurements are acquired in one full spin period (~3 s) but are sampled every 9 s in the high-telemetry mode and every 18 s in low-telemetry modes. High time resolution magnetic field data (16 and four vectors per second in high bit rate and low bit rate sampling, respectively) from the triaxial fluxgate magnetometers on board ISEE 1 [*Russell*, 1978] are averaged over the 3 s resolution of the electron moment data.

Different ion detectors were flown on ISEE 1 specialized for high ion Mach numbers and low ion Mach numbers [*Bame et al.*, 1978]. A detector configured to accurately measure the supersonic solar wind ions on the upstream side of the shock is not well suited to measure the subsonic ions accurately on the downstream side of the shock. The electrons, on the other hand, are subthermal throughout the entire shock layer, and electron moments such as the electron density N_{e} and the flow velocity $\mathbf{U}_{\mathrm{e}}$ can be measured by a single detector through the shock. However, electron measurements are not without problems.

The electron measurements tend to be less accurate than the ion measurements on the upstream side of the shock. Accurate electron moments require accurate determinations of the spacecraft floating potential so that photoelectrons may be excluded. The electron data set used in this paper has been corrected for the spacecraft floating potential using a return current relation similar to that used by *Scudder et al.* [1981] but calibrated with intermittent estimates of spacecraft floating potential. Thus, in the determination of the shock geometry and asymptotic state via a Rankine-Hugoniot analysis, we have approximated the center of mass velocity $\mathbf{U}$ with $\mathbf{U}_{\mathrm{e}}$ realizing that slight slippages are possible and that $\mathbf{U} \approx \mathbf{U}_{\mathrm{e}}$.

3. Shock Asymptotic Parameter Determination

We are interested in $\Delta\Phi^{\mathrm{HT}}$ and its relation to ΔT_{e} and other characteristic shock parameters. The HTF bulk velocity $\mathbf{U}^{\mathrm{HT}}$ is related to the bulk velocity $\mathbf{U}$ in any other frame of reference by the expression $\mathbf{U}^{\mathrm{HT}} \equiv \mathbf{U} + \tilde{\mathbf{V}}^{\mathrm{HT}}$, where the HTF transformation velocity is given by

$$\tilde{\mathbf{V}}^{\mathrm{HT}} = -V_{\mathrm{sh}}\hat{\mathbf{n}} - \frac{\hat{\mathbf{n}} \times [(\mathbf{U}_1 - V_{\mathrm{sh}}\hat{\mathbf{n}}) \times \hat{\mathbf{b}}_1]}{\cos\theta_{Bn1}}. \quad (1)$$

In (1), $V_{\mathrm{sh}}\hat{\mathbf{n}}$, $\mathbf{U}_1$, and $\mathbf{B}_1$ are the shock velocity, upstream bulk velocity, and upstream magnetic field vector, respectively, as viewed in the $\mathbf{U}$ frame of reference. This frame transformation velocity is very sensitive to θ_{Bn1}. Accurate determination of $\tilde{\mathbf{V}}^{\mathrm{HT}}$ requires high-quality determination of the shock geometry and asymptotic state.

The shock geometry and asymptotic parameters for this study have been determined by applying the code developed by *Viñas and Scudder* [1986] with iterative improvement to upstream and downstream ISEE 1 electron moment and magnetic field data intervals. The code gives, in the least squares sense, the best possible determination of the asymptotic state of the shock by optimally solving a subset of the Rankine-Hugoniot jump conditions as constrained by data written in coordinate invariant form:

$$\Delta B_n = \Delta\mathbf{B} \cdot \hat{\mathbf{n}} = 0 \quad (2)$$

$$\Delta G_n = \Delta[\rho(\mathbf{U} - V_{\mathrm{sh}}\hat{\mathbf{n}}) \cdot \hat{\mathbf{n}}] = 0 \quad (3)$$

$$\begin{aligned}\Delta\mathbf{S}_t &= \Delta[\rho(\mathbf{U}\cdot\hat{\mathbf{n}} - V_{\mathrm{sh}})(\mathbf{U}\cdot(\mathbf{1} - \hat{\mathbf{n}}\hat{\mathbf{n}})) \\ &- \frac{\mathbf{B}\cdot\hat{\mathbf{n}}}{4\pi}(\mathbf{B}\cdot(1 - \hat{\mathbf{n}}\hat{\mathbf{n}}))] = 0 \end{aligned} \quad (4)$$

$$\begin{aligned}\Delta\mathbf{E}_t &= \Delta[\hat{\mathbf{n}} \times (\mathbf{U}\cdot(\mathbf{1} - \hat{\mathbf{n}}\hat{\mathbf{n}}))(\mathbf{B}\cdot\hat{\mathbf{n}}) \\ &- (\mathrm{U}\cdot\hat{\mathbf{n}} - V_{\mathrm{sh}})\hat{\mathbf{n}} \times (\mathbf{B}\cdot(\mathbf{1} - \hat{\mathbf{n}}\hat{\mathbf{n}}))] = 0, \end{aligned} \quad (5)$$

where ρ is the plasma mass density, and $\mathbf{B}$ is the magnetic field vector. The variables B_n, G_n, $\mathbf{S}_t$, and $\mathbf{E}_t$ represent the conserved constants of magnetic field intensity along the shock normal, normal mass flux, tangential momentum stress flux vector, and tangential electric field vector, respectively. The Δ is used to denote the change of a physical quantity across the shock (e.g.,

$\Delta X \equiv X_2 - X_1$, where X_1 and X_2 are the upstream and downstream values of a physical quantity X). Least squares solutions to these equations yield $V_{sh}\hat{\mathbf{n}}$, components of the shock normal $\hat{\mathbf{n}}$, and unbiased estimates for the asymptotic Rankine-Hugoniot state parameters such as N_1, $\mathbf{B}_1$, $\mathbf{U}_1$, N_2, $\mathbf{B}_2$, and $\mathbf{U}_2$.

Despite using electron data and all the problems that go with them, Figure 1 illustrates how well the conservation constants are determined for a quasi-perpendicular shock observed by ISEE 1 on December 13, 1977, at 1711:40 UT. The shaded region in each panel indicates the asymptotic shock data intervals used to solve the

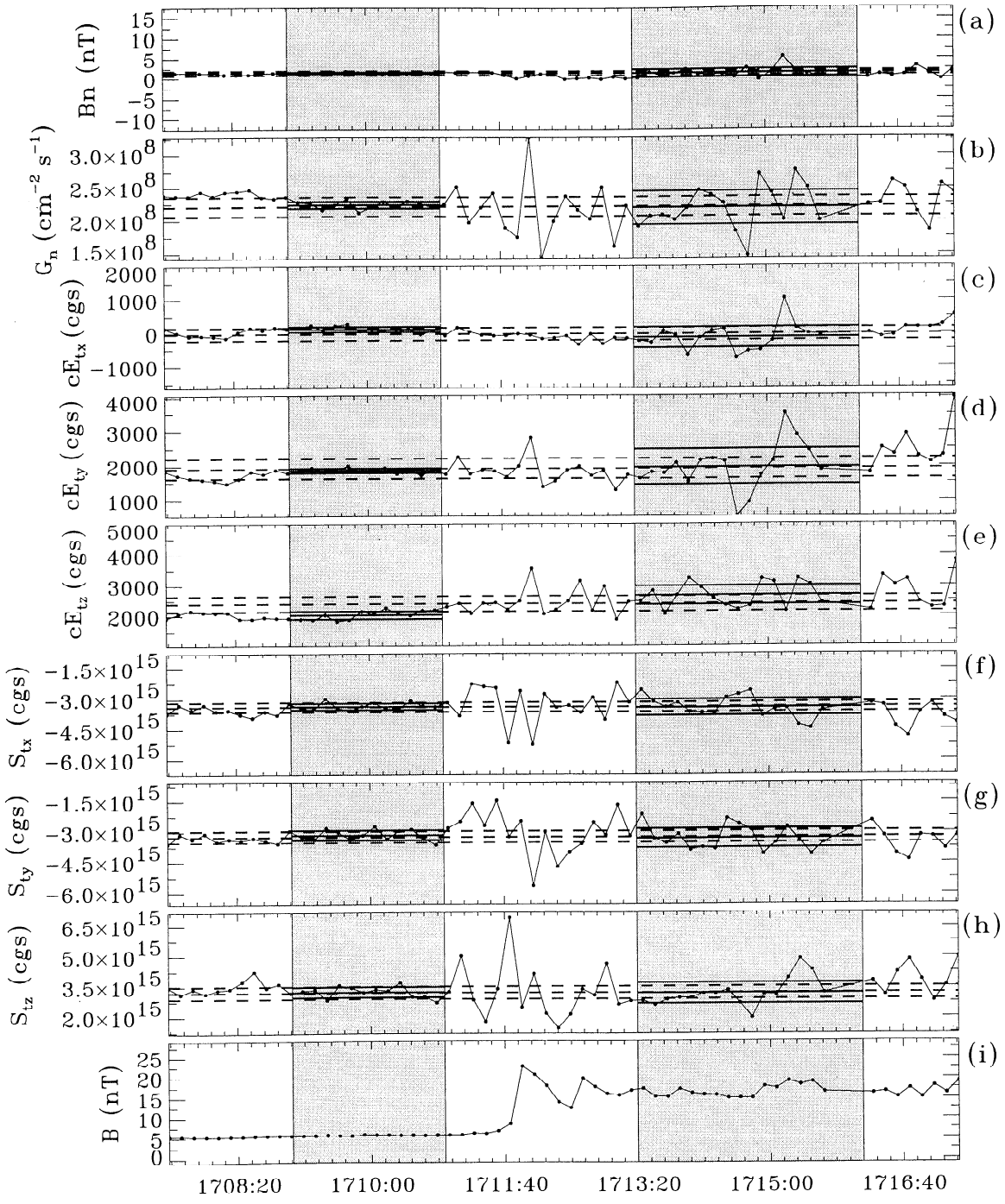

Figure 1. Profiles of the Rankine-Hugoniot constants and magnetic field for a shock event observed by ISEE 1 on December 13, 1977. Shown are (a) the normal component of the magnetic field, (b) the normal mass flux, (c-e) the components of the tangential electric field vector, (f-h) the components of the tangential momentum stress flux vector, and (i) the magnetic field intensity.

Rankine-Hugoniot problem for this shock event. The solid horizontal lines within each of the shaded intervals represent an average over the data in the interval and corresponding uncertainty. The dashed horizontal lines indicate the best fit constant and its estimated uncertainty. Figures 1a–1h clearly demonstrate that the Rankine-Hugoniot constants are well determined asymptotically. The Rankine-Hugoniot constants B_n, G_n, and the components $\mathbf{E}_t$ (to the extent that $\nabla \cdot \mathbf{P}_e$ does not compete with $\mathbf{U}_e \times \mathbf{B}$, where $\mathbf{P}_e$ is the electron pressure tensor) are also found to be conserved inside the shock layer, as expected. The magnetic field intensity profile is provided as a reference in Figure 1i.

The characteristics of the 129 shock macrostates of this new ISEE 1 electron data set as determined by the Rankine-Hugoniot procedure are statistically summarized in Figure 2. The typical upstream electron density N_{e1}, electron temperature T_{e1}, and magnetic field intensity B_1 are found to be 10 ± 6 cm^{-3}, $1.7 \times 10^5 \pm 0.5 \times 10^5$ K, and 9 ± 6 nT, respectively. This data set is predominantly composed of quasi-perpendicular shocks with the typical $\theta_{Bn1} - 63° \pm 16°$. The most probable normal bulk speed $U_{n1} = 300 \pm 60$ km s^{-1}. A fraction of the events are characterized by U_{n1} as high as 600-800 km s^{-1}, which correspond to the high electron temperature increases $\Delta T_e = 100 - 200$ eV discussed in a previous study [*Thomsen et al.*, 1987b]. The electron beta β_e ranges from 0.1 to 15 with a mode of 1.0. In these respects the modal values of upstream parameters are typical of the solar wind at 1 AU [e.g., *Feldman et al.*, 1975]. The downstream-upstream magnetic field B_2/B_1 and density N_2/N_1 ratios are 2.3 ± 0.3 and 2.5 ± 0.3, respectively. The average electron temperature jump is $\Delta T_e = 30 \pm 20$ eV. The Alfvén Mach number is $M_A = U_{n1}\sqrt{4\pi\rho_1}/B_1 = 6 \pm 3$, where ρ_1 is the upstream plasma mass density. The typical upstream electron thermal Mach number is $M_{th} = U_{n1}/V_{the1} = 0.15$, yielding a typical electron HTF thermal Mach number $M_{HTF} = M_{th}/\cos\theta_{Bn1} = 0.3$. *Scudder* [1987] demonstrated that in HTF the electron bulk flow within the shock layer is to a good approximation parallel to the magnetic field in addition to being field-aligned in the asymptotic upstream and downstream sides of the shock. Values of $M_{HTF} \gtrsim 1$ indicate where the field aligned flow approximation used in previous studies [*Scudder et al.*, 1986c; *Scudder*, 1995; *Hull*, 1998] is expected to break down. Because its inertia is no longer negligibly small, the typical electron in this regime has difficulty responding to kinks in the magnetic field and tends to slip magnetic field lines while traversing the shock layer.

4. Empirical Determination of HTF Potential

Determinations of $\Delta\Phi^{HT}$ by direct electric field measurements have only been done for a few shock cases [*Wygant et al.*, 1987]. Part of the problem is that $\Delta\Phi^{HT}$ is the line integral of the weak parallel electric field across the shock, which is difficult, if not impossible, to measure by the standard double-probe electric field measuring techniques.

A good model-free approach to obtaining the HTF potential $\Phi^{HT}(x)$ is to integrate the steady state, electron fluid momentum equation [*Goodrich and Scudder*, 1984] using high time resolution electron moment and magnetic field data through the shock layer (a technique employed only once by *Scudder et al.* [1986b]). Taking advantage of the frame invariance of $\mathbf{E} \cdot \mathbf{B}$, *Goodrich and Scudder* [1984] demonstrated that $\Delta\Phi^{HT}$ can be expressed as

$$\Delta\Phi^{HT} = -\int_{x_1}^{x_2} E_x dx = -\int_{x_1}^{x_2} \frac{E_{||}}{\hat{\mathbf{b}} \cdot \hat{\mathbf{x}}} dx, \qquad (6)$$

which can be simplified [*Scudder et al.*, 1986b] when $d/dt \approx \mathbf{V}_{rel} \cdot \nabla$ to become

$$\begin{aligned} \Delta\Phi^{HT} = \int_{t_1}^{t_2} \Bigg\{ & \frac{1}{eN_e(t)} \frac{dP_{e||}(t)}{dt} \\ & - \frac{[P_{e||}(t) - P_{e\perp}(t)]}{eN_e(t)} \frac{d \ln B(t)}{dt} \\ & + \frac{m_e U_{en}(t)}{e\hat{\mathbf{b}} \cdot \hat{\mathbf{x}}} \hat{\mathbf{b}} \cdot \frac{d\mathbf{U}_e(t)}{dt} - \frac{\eta_{||} J_{||}(t)}{\hat{\mathbf{b}} \cdot \hat{\mathbf{x}}} \Bigg\} dt. \end{aligned} \qquad (7)$$

In (7), $P_{e||}$ and $P_{e\perp}$ are the electron pressure parallel and perpendicular to the magnetic field, $J_{||}$ is the field-aligned current, and $\eta_{||}$ is anomalous resistivity. The first two terms in (7) provide a good estimate of the $\Delta\Phi^{HT}$ across the shock layer provided that the inertial and resistive terms can be neglected as higher-order terms.

Prior to this paper, statistical surveys by *Schwartz et al.* [1988] and *Thomsen et al.* [1987a] used the model-dependent form [*Goodrich and Scudder*, 1984]:

$$\Delta\Phi^{HT} \approx \begin{cases} \frac{\gamma_e}{\gamma_e - 1} \frac{k\Delta T_e}{e} & \gamma_e \neq 1 \\ \frac{k\Delta T_e}{e} \Delta \ln N_e & \gamma_e = 1, \end{cases} \qquad (8)$$

which is valid only to the extent an electron polytrope law $P_e \propto N_e^{\gamma_e}$ (where γ_e is the effective electron polytrope index) is known to be valid through the shock layer.

An alternative model-free method to determining $\Delta\Phi^{HT}$ is to use the time stationary, electron fluid energy equation in the frame-independent form [*Boyd and Sanderson*, 1969]:

$$\begin{aligned} \nabla \cdot \Big(\mathbf{q}_e + \frac{1}{2} \mathrm{Tr}\mathbf{P}_e \mathbf{U}_e + \mathbf{P}_e \cdot \mathbf{U}_e + \frac{m_e N_e U_e^2 \mathbf{U}_e}{2} \\ - eN_e \Phi \mathbf{U}_e \Big) = S + \mathbf{U}_e \cdot \mathbf{R} \end{aligned} \qquad (9)$$

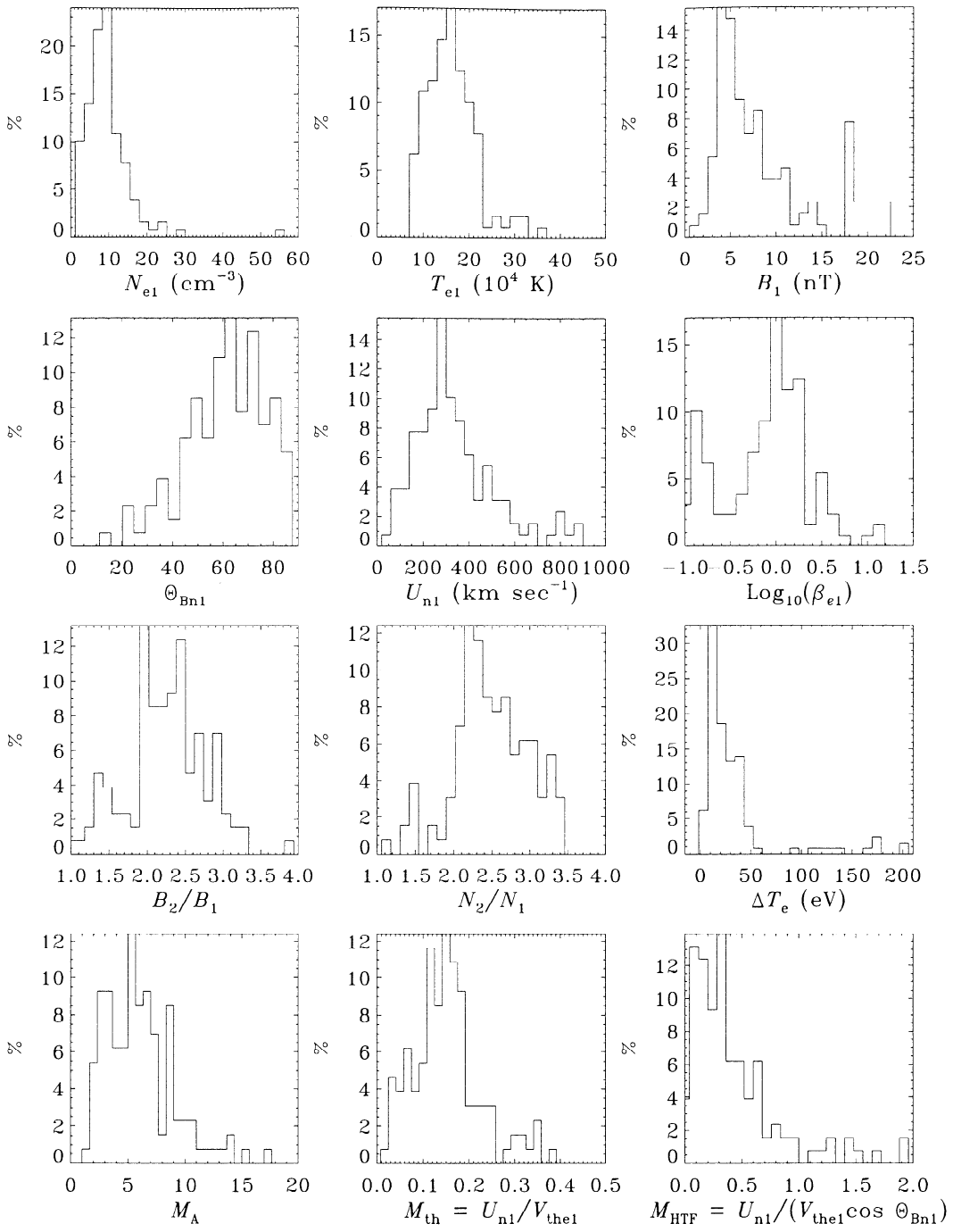

Figure 2. Histograms summarizing the macrostate of the shocks used in the study.

where $\mathbf{q}_e$ is the electron heat flux vector, $\mathbf{P}_e$ is the electron pressure tensor, and Φ is determined from $\mathbf{E} = -\nabla\mathbf{\Phi}$. The parameters $\mathbf{R}$ (often modeled as $eN_e\boldsymbol{\eta}\cdot\mathbf{J}$, where J is the current and $\boldsymbol{\eta}$ is the anomalous resistivity tensor) and S represent a source or sink of momentum and energy, respectively, as caused by wave-particle interactions. Integrating (9) across a 1-D planar layer in HTF under the assumption that the wave-particle terms are negligible results in the following expression for the HTF potential jump:

$$\Delta\Phi^{HT} = \frac{1}{e}\Delta\left[\frac{q_{||}}{N_eU_e^{HT}} + k\left(\frac{3}{2}T_{e||} + T_{e\perp}\right) + \frac{m_eU_e^{HT\,2}}{2}\right] + O\left(\frac{\int_{-\infty}^{\infty}(S + \mathbf{U}_e^{HT}\cdot\mathbf{R})dx}{eN_eU_e^{HT}}\right), \quad (10)$$

where $T_{e||}$ and $T_{e\perp}$ represent the electron temperature parallel and perpendicular to the magnetic field and $U_e^{HT} = U_n/\cos\theta_{Bn}$ is the magnetic field aligned elec-

tron bulk speed in HTF, with U_n being the asymptotic flow velocity along the shock normal. The advantage of using (10) is that the $\Delta\Phi^{HT}$ is determined from the difference between upstream and downstream states (as long as contributions from $\mathbf{R}$ and S can be neglected), as opposed to a sum of all of the contributions connecting the upstream and downstream states. Thus the cumulative errors of quadrature in the determination of the potential are dramatically reduced, in principle. However, (10) does require the electron heat flux, a higher-order moment that is not so accurately measured, as well as a priori knowledge that S and $\mathbf{R}$ terms are not important. In the present paper, both (7) and (10) are used to determine $\Delta\Phi^{HT}$ for 129 Earth bow shock events observed by ISEE 1, a hundredfold increase in our model-free knowledge of $\Delta\Phi^{HT}$ at collisionless shocks.

5. Observations

Plate 1 compares the change in the HTF potential $\Delta\Phi^{HT}_{MOM}$ determined by integrating the momentum equation with the change in HTF potential $\Delta\Phi^{HT}_{EN}$ determined from the electron energy equation using asymptotic Rankine-Hugoniot parameters. The error bars in $\Delta\Phi^{HT}_{MOM}$ represent the estimated cumulative errors associated by integrating (7) across the layer, whereas the error bars in $\Delta\Phi^{HT}_{EN}$ are the propagated uncertainties associated with the averaged asymptotic parameters used to determine $\Delta\Phi^{HT}_{EN}$. Note, however, that no estimates of systematic error of setting $S, \mathbf{R} = 0$ are included. The best fit slope suggests that $\Delta\Phi^{HT}_{EN}$ is roughly 20% larger than $\Delta\Phi^{HT}_{MOM}$; however, unity slope cannot be ruled out because of the large uncertainties associated with $\Delta\Phi^{HT}_{MOM}$.

Figures 3a–3d show where the results of two methods used to compute $\Delta\Phi^{HT}$ differ the most for the strong shock observed on November 7, 1977, by ISEE 1 considered by *Scudder et al* [1986a, b, c]. Figure 3a depicts the incremental changes in the HTF potential through the shock layer determined from the momentum equation $\delta\Phi^{HT}_{MOM}$ versus the changes determined from the energy equation $\delta\Phi^{HT}_{EN}$. Although there are a few exceptions, $\delta\Phi^{HT}_{EN}$ and $\delta\Phi^{HT}_{MOM}$ show strong agreement to within the estimated uncertainty. The consistency between the two different determinations is suggested by the histogram of $\delta\Phi^{HT}_{EN} - \delta\Phi^{HT}_{MOM}$ weighted by the estimated uncertainty illustrated in Figure 3b. All of the points are within 2σ of zero, which indicates that the two methods are equivalent. However, the largest discrepancy between the two methods appears to be in the magnetic ramp region as shown in Figure 3c, which depicts the time evolution of $\delta\Phi^{HT}_{EN} - \delta\Phi^{HT}_{MOM}$. The profiles of Φ^{HT}_{EN} (solid line) and Φ^{HT}_{MOM} (dashed line) are provided in Figure 3d as a reference. Evidently, the two profiles are coincident until about ~2251:30 UT, where Φ^{HT}_{EN} becomes larger than Φ^{HT}_{MOM}. The potential jumps $\Delta\Phi^{HT}_{EN}$ and $\Delta\Phi^{HT}_{MOM}$ estimated from the upstream and downstream shaded regions in Figure 3c to be 62±3 eV and 49 ± 34 eV, respectively, are consistent with one another. However, the mean value of $\Delta\Phi^{HT}_{EN}$ is larger than that of $\Delta\Phi^{HT}_{MOM}$ for this shock example, a trend that is characteristic of this shock data set, as evidenced in Plate 1. Part of the discrepancy between the two methods could be explained by the different mix of fluid quantities used to determine $\Delta\Phi^{HT}$. The energy equation determination depends on the electron heat flux, a third moment of the electron velocity distribution function, which is difficult to measure, while the momentum equation form does not. Integration of (7) to get the cross-shock potential jump does, however, require the integrand to be sufficiently resolved throughout the shock layer to perform the numerical integration. This may not be the case in the shock ramp region, where the electron moment and the magnetic field gradients are largest and aliasing is most troublesome. Moreover, wave-particle effects ($S, \mathbf{R}$) may not be negligible as has been assumed, especially in the main magnetic ramp where currents are largest.

Detailed comparisons of data through each shock layer suggest that the electron density and electron temperature may be related via a polytrope law [*Hull*, 1998], which means that (8) can be used to compute $\Delta\Phi^{HT}$. The parameter γ_e for each shock event in this study is determined by a two-parameter fit to $\ln T_e(t)$ and $\ln N_e(t)$ through the shock layer. The choice of an appropriate time interval of moment data for a good determination of γ_e is somewhat arbitrary. We chose the time interval that yielded the best corroboration within the estimated uncertainty between the two-parameter-fit method and the following two alternative approaches used to compute the electron polytrope index: (1) a one-parameter fit to incremental changes $\delta \ln T_e$ and $\delta \ln N_e$ between successive data points through the layer and (2) a one-parameter linear fit to $\delta\Phi^{HT}$ and δT_e (see *Hull* [1998] for details). The typical γ_e determined from the two-parameter fit method is 2.4 ± 0.8.

Plate 2a compares $\Delta\Phi^{HT}_{MOM}$ with the polytrope estimate $\Delta\Phi^{HT}_{\gamma}$. A linear regression analysis suggests that $\Delta\Phi^{HT}_{MOM}$ is consistent with $\Delta\Phi^{HT}_{\gamma}$, though $\Delta\Phi^{HT}_{MOM}$ begins to depart from $\Delta\Phi^{HT}_{\gamma}$ at higher values. The fact that $\Delta\Phi^{HT}_{MOM}$ is consistent with $\Delta\Phi^{HT}_{\gamma}$ suggests that integrating the electron momentum equation across the shock layer is more accurate than what is implied by the cumulative errors. In contrast, Plate 2b shows that $\Delta\Phi^{HT}_{EN}$ is roughly 30% larger than $\Delta\Phi^{HT}_{\gamma}$. For the shocks treated in this study we found $\Delta\Phi^{HT}_{EN} \approx (5k/2e)\Delta T_e$. The heat flux and the inertial terms tended to cancel each other, and the anisotropy was usually small in (8). The relationship between $\Delta\Phi^{HT}_{EN}$ and ΔT_e implies an electron polytrope index $\gamma_e = 5/3$, which is inconsistent with the N_e-T_e relationship observed within the shock layer. The source of the uncertainty is difficult to ascertain. Because it is most consistent with the data, $\Delta\Phi^{HT}_{MOM}$ will be used instead of $\Delta\Phi^{HT}_{EN}$ in the compar-

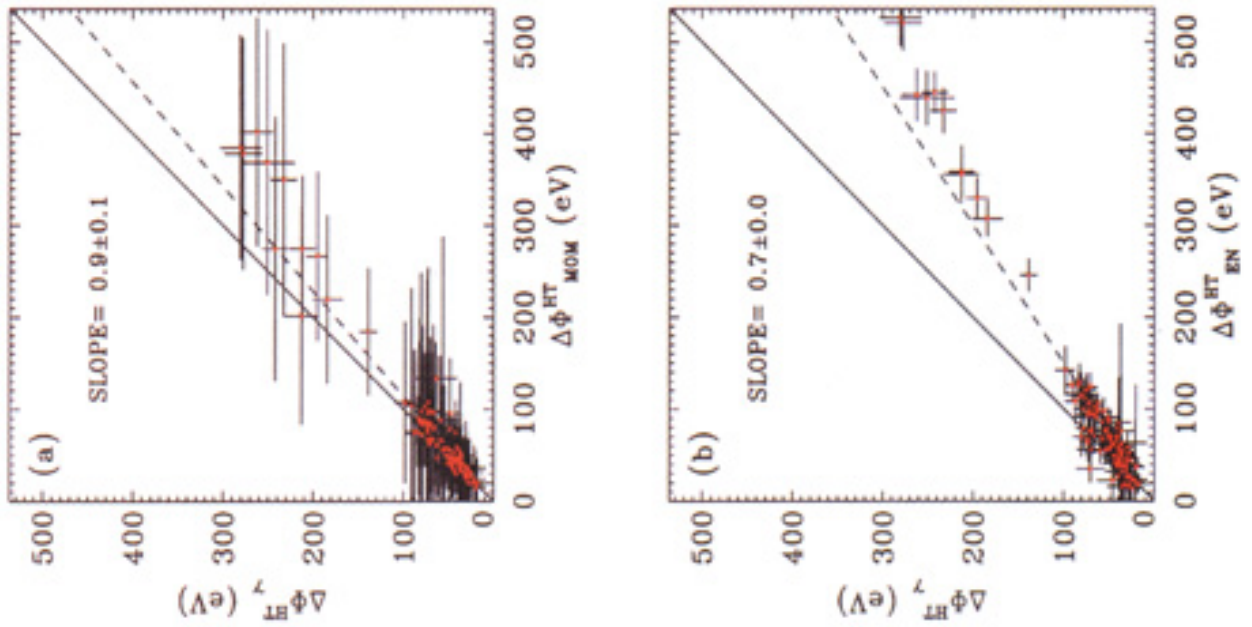

Plate 2. Scatterplots of (a) $\Delta\Phi^{HT}_{\gamma}$ versus $\Delta\Phi^{HT}_{MOM}$ and (b) $\Delta\Phi^{HT}_{\gamma}$ versus $\Delta\Phi^{HT}_{EN}$.

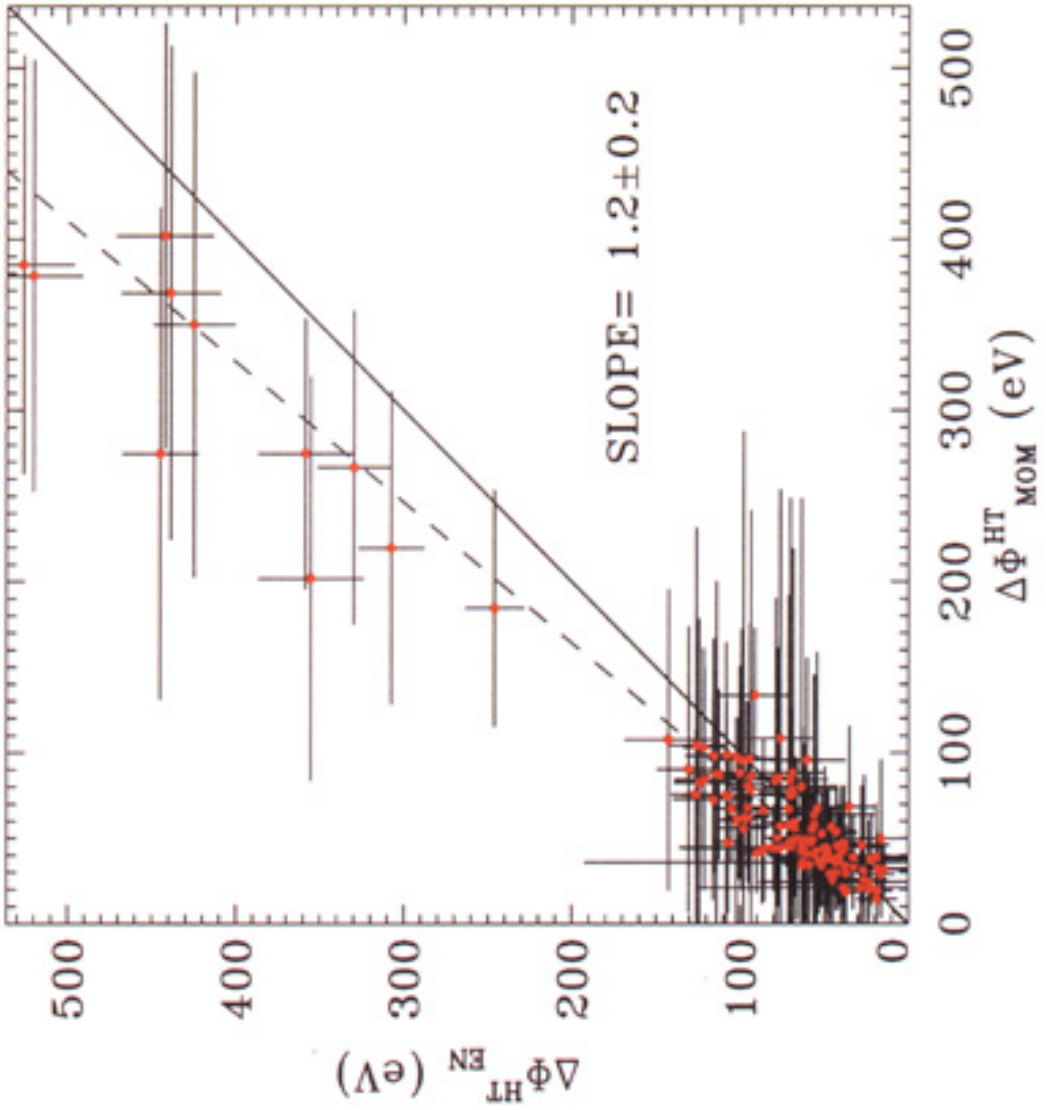

Plate 1. Comparison of $\Delta\Phi^{HT}_{MOM}$ determined by integrating the momentum equation and $\Delta\Phi^{HT}_{EN}$ determined from the electron energy equation.

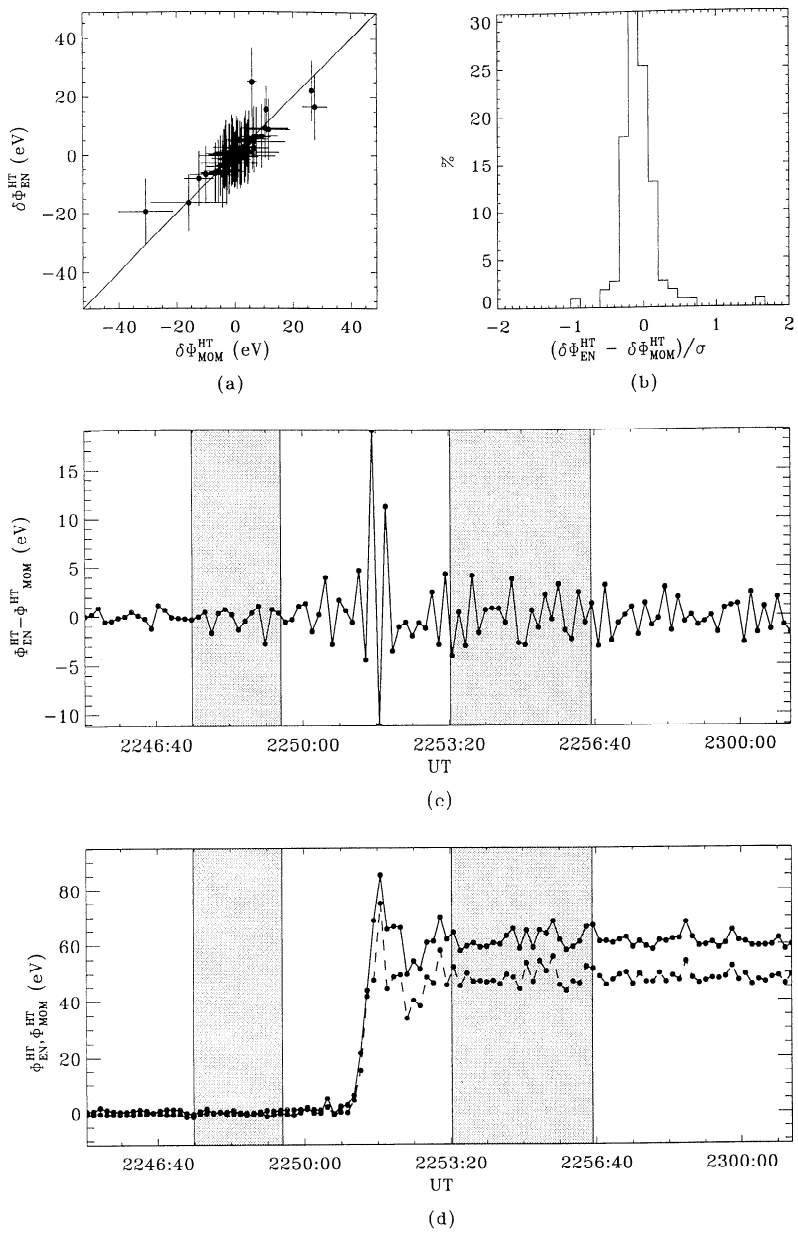

Figure 3. (a) Scatterplots of $\delta\Phi^{\rm HT}_{\rm MOM}$ versus $\delta\Phi^{\rm HT}_{\rm EN}$, (b) histogram of $\delta\Phi^{\rm HT}_{\rm EN} - \delta\Phi^{\rm HT}_{\rm MOM}$ weighted by the estimated uncertainty, (c) $\delta\Phi^{\rm HT}_{\rm EN} - \delta\Phi^{\rm HT}_{\rm MOM}$ versus time, and (d) $\Phi^{\rm HT}_{\rm EN}$ (solid line) and $\Phi^{\rm HT}_{\rm MOM}$ (dashed line) profiles for the November 7, 1977, bow shock crossing.

isons with other shock macroscopic parameters. Thus in the remainder of the paper we will adopt the notation $\Delta\Phi^{\rm HT} \equiv \Delta\Phi^{\rm HT}_{\rm MOM}$ when referring to the HTF potential jump.

The relationship between the change in the HTF potential $\Delta\Phi^{\rm HT}$ and the change in the normal component of the ion ram energy $\Delta(m_{\rm p}U_{\rm n}^2/2)$ is summarized in Plate 3a. The color code in Plate 3a indicates the θ_{Bn1} dependence. Plate 3b and Plate 3c show the same correlation as displayed in Plate 3a, except the colors indicate the dependence of the correlation on the upstream electron beta $\beta_{\rm e1}$ and $M_{\rm HTF}$, respectively. A linear fit to the data resulted in the following:

$$\Delta\Phi^{\rm HT}({\rm eV}) = -121^{+8}_{-13}\Delta(m_{\rm p}U_{\rm n}^2/2)({\rm keV}). \qquad (11)$$

Only data points (squares) with a relative uncertainty $\lesssim 0.5$ in $|\Delta(m_{\rm p}U_{\rm n}^2/2)|$ were used in the fit. The shock events (triangles) corresponding to small values of $|\Delta(m_{\rm p}U_{\rm n}^2/2)|$ are associated with much larger relative uncertainties and are believed to be suspect for two reasons: (1) The electron flow speeds used to compute $\Delta(m_{\rm p}U_{\rm n}^2/2) = m_{\rm p}/m_{\rm e}(\Delta m_{\rm e}U_{\rm ne}^2)$ for these suspicious shock cases approach the VES instrument's capability to detect, and (2) the suspect shock events are characterized by fluctuations comparable to the time stationary background plasma and field properties as indicated

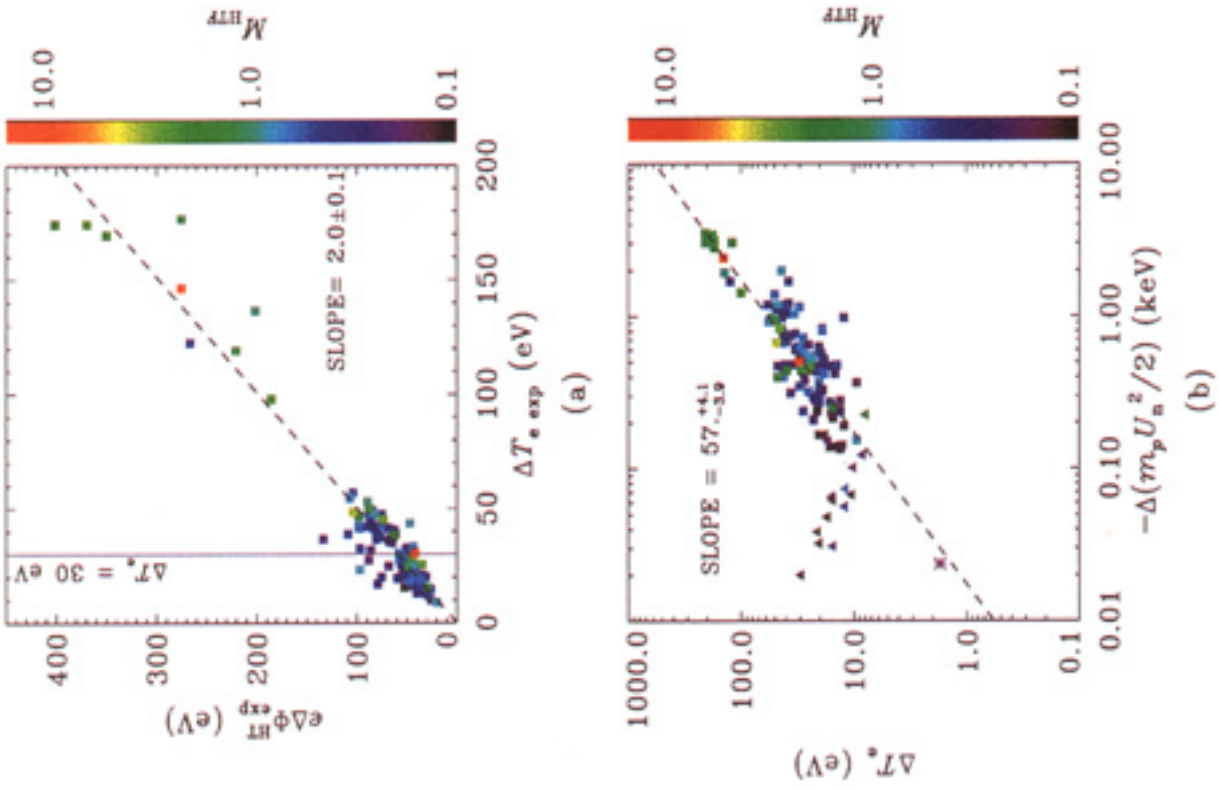

Plate 4. Scatterplots of (a) ΔT_e and $\Delta\Phi^{HT}$ and (b) $-\Delta(m_p U_n^2/2)$ and ΔT_e across 130 Earth bow shocks observed by ISEE 1. The color code depicts M_{HTF}.

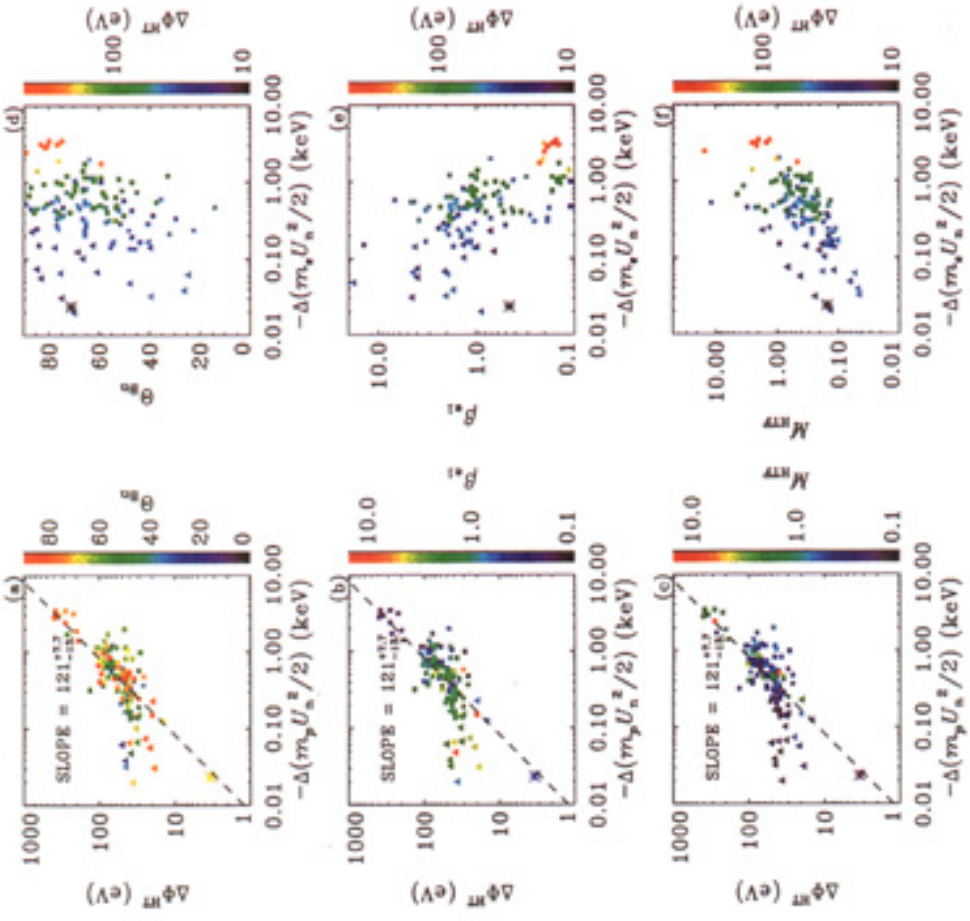

Plate 3. Scatterplots of $\Delta\Phi^{HT}$ versus $-\Delta(m_p U_n^2/2)$ color-coded to depict (a) θ_{Bn1}, (b) β_{e1}, and (c) M_{HTF} dependence. The scatterplots of $-\Delta(m_p U_n^2/2)$ and θ_{Bn1} (Plate 3d), $-\Delta(m_p U_n^2/2)$ and β_{e1} (Plate 3e), and $-\Delta(m_p U_n^2/2)$ and M_{HTF} (Plate 3f) are color-coded to indicate dependence on $\Delta\Phi^{HT}$.

by the higher values of β_{e1} (see Plate 3b), resulting in aliased electron moment quantities. It is not clear that the trend in $\Delta\Phi^{HT}$ with respect to $\Delta(m_p U_n^2/2)$ should depart from the linear correlation suggested by the moderate to strong shock examples as the change in the flow energy goes to zero. A very weak shock case ($M_f = U_{ne1}/C_{f1} \approx 1.2$, $B_2/B_1 \approx 1.3$, where M_f is the upstream fast mode Mach number and C_{f1} represents the upstream fast mode speed) observed by Galileo and discussed by *Hull et al.* [1998] is indicated by the color-coded asterisks in Plates 3a–3f. The $\Delta\Phi^{HT}$ for this weak shock case was more accurately determined using leverage of the full 3-D upstream and downstream electron velocity distribution functions. A parameter that distinguishes the Galileo weak shock event from the ISEE 1 weak shock observations is the upstream electron β_{e1}. The parameter β_{e1} for the Galileo event was estimated to be 0.46, whereas $\beta_{e1} \gtrsim 1$ for the ISEE 1 weak shock examples. Consequently, the observed magnetic field and plasma properties across this weak shock event are more laminar in comparison with the ISEE 1 weak shock observations. The weak shock temperature measurements and potential jump determinations suggest that the linear trend should continue into the lower flow energy limit, though more statistics in this limit are needed to clarify these results.

A complementary view of the relationship between $\Delta\Phi^{HT}$ (indicated by the color) and the upstream parameters β_{e1}, θ_{Bn1}, and M_{HTF} is provided in Plates 3d–3f. The high values of $\Delta\Phi^{HT}$ in our data set are typically characterized by high θ_{Bn1}, low β_{e1}, and consequently high values of M_{HTF}, whereas the low values of $\Delta\Phi^{HT}$ are characterized by high β_e and lower values of M_{HTF} with no apparent dependence on θ_{Bn1}. *Thomsen et al.* [1987b] established that ΔT_e was strongly correlated with $\Delta(m_p U_n^2/2)$ and suggested that this first-order dependence should be normalized out on future studies of ΔT_e. *Schwartz et al.* [1988] concluded that the model-dependent normalized potential jump $\Delta\Phi^{HT}/|\Delta(m_p U_n^2/2)|$ (with $\Delta\Phi^{HT} \propto \Delta T_e$) did not seem to be organized by any of the standard upstream parameters such as bow shock model determined geometry, plasma beta, or electron to ion temperature ratios. However, $\Delta\Phi^{HT}$ and $\Delta(m_p U_n^2/2)$ are not strictly proportional, as suggested in Plate 3, and such a normalization scheme could result in misleading conclusions on the behavior of $\Delta\Phi^{HT}$ and other asymptotic parameters. A possibility remains that the trends implied by Plates 3a–3f are artifacts of biases characteristic of the data set.

Plate 4a compares the electron temperature change ΔT_e with the change in the HTF potential $\Delta\Phi^{HT}$. The color code represents the dependence of the correlation with respect to M_{HTF}. The typical change in electron temperature $\Delta T_e \approx 30 \pm 20$ eV is indicated by the vertical solid line in Plate 4a. Our present data set also includes some of the shock examples with unusually large electron temperature jumps featured in earlier studies [*Thomsen et al.*, 1987b; *Schwartz et al.*, 1988]. The plot shows that ΔT_e is for the most part linearly related to $\Delta\Phi^{HT}$ with a slope $\langle\alpha\rangle = 2.0 \pm 0.1$. The events corresponding to $M_{HTF} = U_{e1}^{HT}/V_{the1} \gtrsim 1$ are in the regime where the field-aligned flow [*Scudder*, 1987] approximation breaks down. The proportionality is suggestive of a polytrope with $\langle\gamma_{eff}\rangle = \langle\alpha\rangle/(\langle\alpha\rangle - 1) = 2.0 \pm 0.1$ that is consistent with the most probable $\gamma_e = 2.4 \pm 0.8$ determined from fits to $N_e(t)$ and $T_e(t)$ [*Hull*, 1998]. However, if $\langle\gamma_{eff}\rangle = 2.0 \pm 0.1$, then that implies an upper bound on the electron temperature ratio $T_{e2}/T_{e1} < 4^{\langle\gamma_{eff}\rangle - 1} \sim 4$ (assuming a maximum compression ratio of 4), which is considerably less than the larger observed values of $T_{e2}/T_{e1} \sim 10$. The more extreme values of T_{e2}/T_{e1} can be explained by a polytrope if you allow for a range of $\langle\gamma_{eff}\rangle$ as found in the fits to $\ln T_e(t)$ and $\ln N_e(t)$ [*Hull*, 1998].

Plate 4b illustrates the correlation between ΔT_e and $\Delta(m_p U_n^2/2)$ using the same format as Plate 3c. A linear fit ΔT_e and $-\Delta(m_p U_n^2/2)$ using only the data points (squares) with a relative uncertainty $\lesssim 0.5$ in $\Delta(m_p U_n^2/2)$ yields

$$\Delta T_e(\mathrm{eV}) = -(57 \pm 4)\Delta(m_p U_n^2/2)(\mathrm{keV}). \qquad (12)$$

The correlation between ΔT_e and $\Delta(m_p U_n^2/2)$ is not surprising in light of the linear relation between ΔT_e and $\Delta\Phi^{HT}$. Nevertheless, the trend suggests that ΔT_e is a coherent process even for $\Delta T_e \gtrsim 100$ eV and is also in substantial qualitative agreement with the results of earlier studies [*Thomsen et al.*, 1987b; *Schwartz et al.*, 1988].

6. Empirical Evidence of $\Delta\Phi^{HT} = \kappa\Delta B$

Comparisons between the magnetic field strength $B(x)$ and the de Hoffmann-Teller potential $\Phi^{HT}(x)$ profiles suggest that they are correlated. Evidence of such a correlation at a shock observed by ISEE 1 at ~1751 UT on December 13, 1977, is illustrated in Figure 4. The top panel is a comparison between $B(x)$ (solid line) and $\Phi^{HT}(x)$ (dashed line). The $\Phi^{HT}(x)$ tracks $B(x)$ quite well throughout the shock layer, exhibiting the same overshoot-undershoot structure of the magnetic field which is characteristic of supercritical shocks. The bottom panel in Figure 4 shows a scatterplot of the incremental changes δB and $\delta\Phi^{HT}$ through the layer. These figures suggest that the δB are proportional to $\delta\Phi^{HT}$ with $\kappa \approx 7$. The fact that δB are proportional to $\delta\Phi^{HT}$ implies that the total change in the de Hoffmann-Teller potential may be related to the total change in the magnetic field as $\Delta\Phi^{HT} = \kappa\Delta B$, where κ is a constant for a given shock layer.

A reasonable test of the validity of a relationship between δB and $\delta\Phi^{HT}$ is to compare $\kappa(\delta\phi^{HT}, \delta B)$ determined from a linear regression analysis to the incremental changes δB and $\delta\Phi^{HT}$ through each shock layer with the $\kappa(\Delta\Phi^{HT}, \Delta B)$ determined from the total

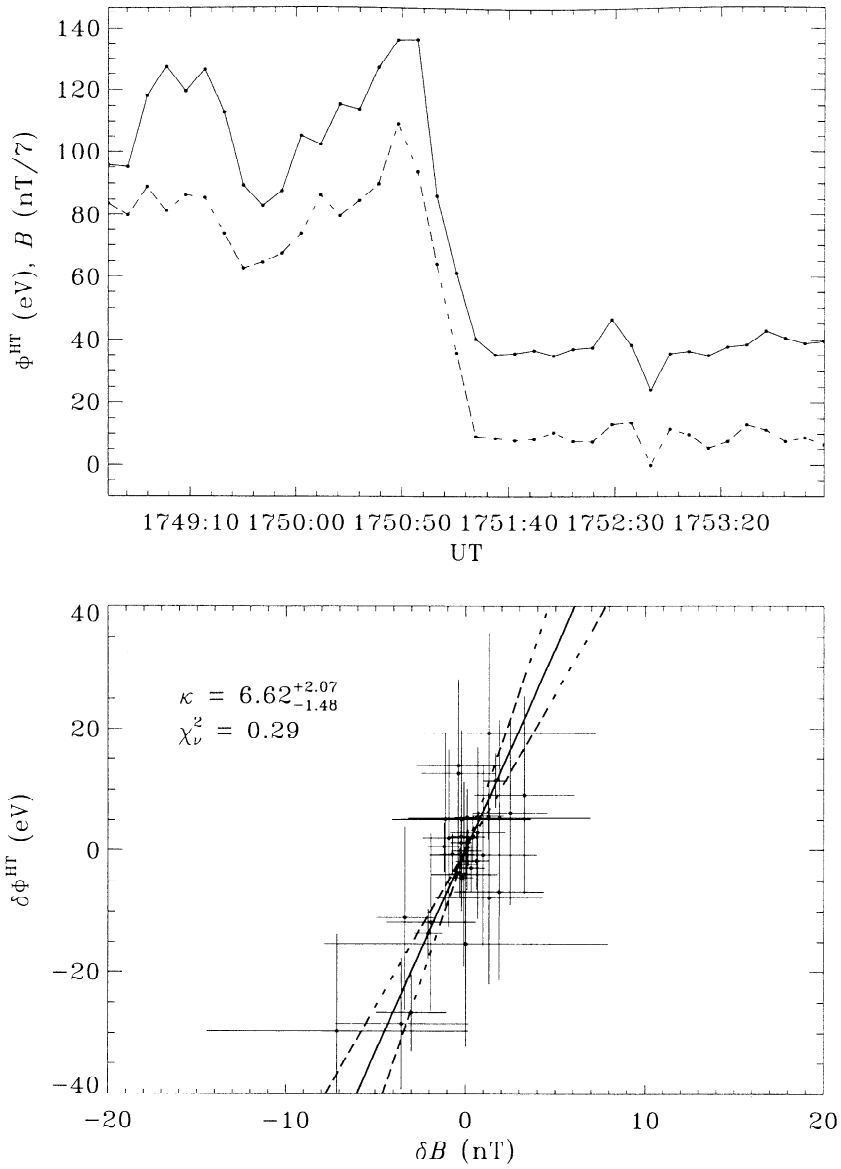

Figure 4. Magnetic field intensity (solid line) and de Hoffmann-Teller potential (dashed line) profiles of an ISEE 1 bow shock crossing on December 13, 1977, are illustrated in the top panel. The magnetic field in the top panel is rescaled for the purpose of comparison. The bottom panel is a scatterplot of $\delta\Phi^{HT}$ and δB for the shock event.

jumps $\Delta\Phi^{HT}$ and ΔB across the shock, as is depicted in Figure 5. Internal consistency requires $\kappa(\delta\phi^{HT}, \delta B)$ to be equal to $\kappa(\Delta\Phi^{HT}, \Delta B)$. Although a fair number of the shocks in the data set are internally consistent, the best fit slope of 1.5 (indicated by the dashed line) suggests that a number of the shock observations are not. However, a closer inspection of the distribution of reduced χ^2 reveals that the issue is time stationarity. Figure 6a gives the reduced chi-square χ^2_ν distribution obtained from the fits to δB and $\delta\phi$ for each shock. The χ^2_ν distribution function is bimodal, with the better determined fits having $\chi^2_\nu < 1.0$. A measure of stationarity is the β_e, which is contrasted with χ^2_ν in Figure 6b. Figure 6b demonstrates that the χ^2_ν depends on β_e, with the better determined fits being associated with $\beta_e \lesssim 1$. Using a cutoff of $\chi^2 \leq 1.5$, we found $\kappa(\delta\phi^{HT}, \delta B)$ to be consistent with $\kappa(\Delta\Phi^{HT}, \Delta B)$.

It is not obvious that such a relation should exist for collisionless, fast mode shocks, although such a relation between the changes in the magnetic field and the changes in the potential in plasmas has been derived in an earlier study [*Whipple*, 1977]. In *Whipple*'s [1977] general approach the electrons and ions are both assumed to be magnetized. *Whipple* [1977] then enforces quasi-neutrality to derive an expression relating the potential to the magnetic field by differentiating with respect to position along the field line. However, at collisionless shocks the length scale that characterizes the variation of the magnetic field intensity is intermediate between the electron skin depth and the ion

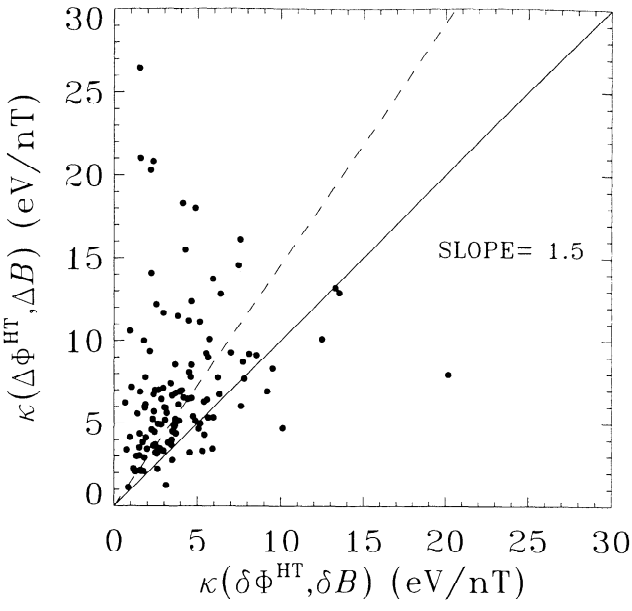

Figure 5. Comparison of the proportionality constant $\kappa(\delta\phi^{\mathrm{HT}}, \delta B)$ determined by performing a linear regression analysis to the incremental changes δB and $\delta\Phi^{\mathrm{HT}}$ through the layer with the $\kappa(\Delta\Phi^{\mathrm{HT}}, \Delta B)$ determined from the jump in the de Hoffmann-Teller potential and magnetic field across the shock.

skin depth. As a result, the electrons are magnetized everywhere throughout the shock, while the ions are not. Nevertheless, the leverage of Whipple's analysis was that of quasi-neutrality ($L_{\mathrm{sh}} \gg \lambda_{\mathrm{De}}$); it still suggests that there will be such a relation even though the ions are not magnetized.

That there must be a relationship between δB and $\delta\Phi^{\mathrm{HT}}$ can be motivated by arguments based on the zero normal current condition required for time stationary, planar shock layers. Zero normal current requires the electron normal flux (current) to balance ion normal flux (current). However, electrons, being magnetized, can be mirrored by the increasing magnetic field, whereas most of the ions, because of their large gyroradius, tend to jump across the layer (only a small fraction of the ions get reflected by the shock). The different inertial responses of electrons and ions to the shock field structure result in a parallel electric field which acts as a feedback mechanism that counters electron mirroring and accelerates the bulk of the electrons to maintain a steady state of equal electron and ion normal number fluxes through the shock layer. Thus an increase in the HTF potential coincides with an increase in the magnetic field intensity. Otherwise a normal current would develop, and the shock would not be stationary. A large fraction of the electron population must get through in order for the electron and ion normal number fluxes to be equal; therefore we believe that κ should scale as $O\left(kT_{e\perp}/(eB)\mid_{sw}\right)$ (see model prediction discussed by *Hull* [1998]).

7. Conclusions

The $\Delta\Phi^{\mathrm{HT}}$ was computed via three different techniques. The energy equation determination of $\Delta\Phi^{\mathrm{HT}}$ was systematically higher than the other two consistent determinations obtained by integrating the momentum equation and by the polytrope relation, respectively. The source of the discrepancy is difficult to ascertain. The largest discrepancy between the two methods occurs in the shock magnetic ramp, where the integrand of (7) is most uncertain because of aliasing effects on the measurements due to the large gradients and where the current is largest, which may give rise to nonnegligible contributions from the wave-particle terms neglected in

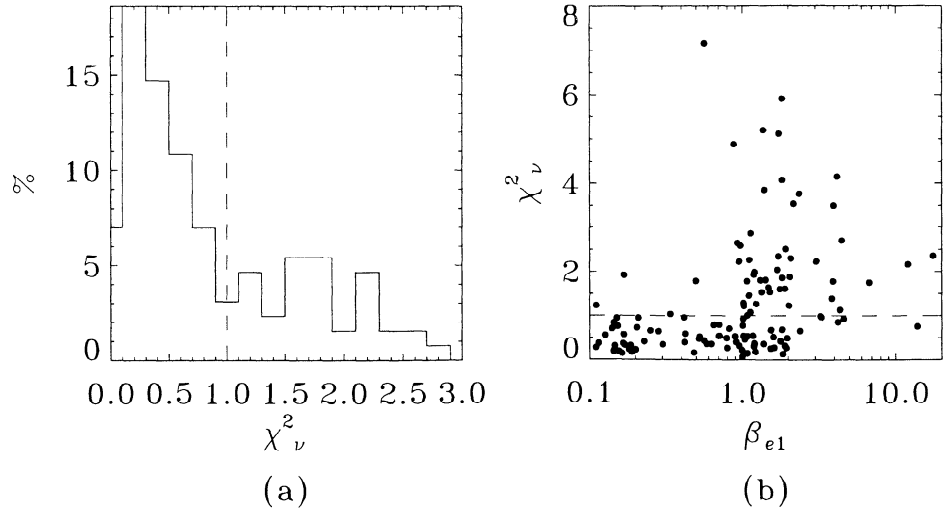

Figure 6. (a) Distribution of χ^2_ν associated with $\kappa(\delta\phi^{\mathrm{HT}}, \delta B)$ determinations. (b) Comparison of χ^2_ν with β_e.

the determination of $\Delta\Phi^{HT}_{MOM}$ and $\Delta\Phi^{HT}_{EN}$ from (7) and (10). Moreover, $\Delta\Phi^{HT}_{EN}$ depends on the electron heat flux, a higher-order moment that is difficult to measure.

Using the momentum equation determined $\Delta\Phi^{HT}$, we recover the correlation of $\Delta\Phi^{HT}$ and ΔT_e with $\Delta(m_p U_n^2/2)$ discussed in earlier experimental surveys [*Thomsen et al.*, 1987b; *Schwartz et al.*, 1988]. The trends appear to be linear at moderate to large values of $\Delta(m_p U_n^2/2)$. Moment data of high quality are needed to clarify the limit of small $\Delta(m_p U_n^2/2)$.

We find $\Delta\Phi^{HT}$ to be proportional to ΔT_e, suggesting a polytrope with an effective polytrope index $\langle\gamma_{eff}\rangle = 2.0 \pm 0.1$ that is consistent with the typical $\gamma_e = 2.4 \pm 0.8$ determined by fits to $N_e(t)$ and $T_e(t)$ [*Hull*, 1998]. However, $\langle\gamma_{eff}\rangle \approx 2$ cannot explain the downstream-upstream electron temperature ratios greater than 4. The more extreme electron temperature ratios can be explained by a polytrope if you allow for a range of polytrope indices, as found in observations [*Hull*, 1998]. Thus $\langle\gamma_{eff}\rangle \approx 2$ probably reflects the biases associated with the limited conditions that define the shocks in our data set.

We provided empirical support for the notion that the incremental changes δB are proportional to $\delta\Phi^{HT}$ through the layer, with a proportionality constant κ that is assumed to be a fixed constant [*Hull et al.*, 1998]. The fact that δB are proportional to $\delta\Phi^{HT}$ implies that the HTF potential distribution through the layer is linearly related to the magnetic field intensity profile. Such a relationship drastically simplifies the determination of electron accessibility to regions within the shock layer from the boundaries that define the shock system [*Hull et al.*, 1997; *Hull*, 1998], which is relevant to theoretical studies [*Hull et al.*, 1998; *Hull*, 1998] of the effects of the shock dc electric and magnetic fields on dispersing the electron velocity distribution function and hence changing the electron temperature as the electrons traverse the shock layer.

The work of this paper provides a better understanding of the interconnections between the various fluid electron trends across collisionless, fast mode shocks as may be governed by the shock macroscopic electric and magnetic fields. The incident ram energy is central to the formation and the strength of the shock. As $m_p U_{n1}^2/2$, increases the magnetic field and plasma get more compressed. The increase in ΔB coincides with an increase in $\Delta\Phi^{HT}$ so as to preserve zero normal current and quasi-neutrality. The correlation between $\Delta\Phi^{HT}$ and ΔB provides a link between what energy gets extracted from the flow, $-\Delta(m_p U_n^2/2)$, and what goes into nondirected energy, ΔT_e, which was missing in previous studies [*Thomsen et al.*, 1987b; *Schwartz et al.*, 1988]. The mechanism responsible for this conversion of directed electron energy is believed to be the cross-shock potential $\Delta\Phi^{HT}$, which when combined with the effect of the magnetic field (on magnetized electrons) broadens the electron distribution and thereby reversibly changes the electron temperature in lowest order, as suggested in previous studies [e.g., *Goodrich and Scudder*, 1984; *Scudder*, 1995; *Hull et al.*, 1998].

Acknowledgments. This work was submitted in partial fulfillment of the requirements for the Ph.D. in physics in the Graduate College of the University of Iowa [*Hull*, 1998]. Support for this research for A.J.H. was provided by the GSRP fellowship program under NASA grant NGT-70411. The work at UCLA was supported by a grant from the Institute of Geophysics and Planetary Physics, Los Angeles.

Michel Blank thanks Goetz Paschmann and another referee for their assistance in evaluating this paper.

References

Bame, S. J., J. R. Asbridge, H. E. Felthauser, J. P. Glore, G. Paschmann, P. Hemmerich, K. Lehmann, and H. Rosenbauer, ISEE-1 and ISEE-2 fast plasma experiment and the ISEE-1 solar wind experiment, *IEEE Trans. Geosci. Electron.*, *16*(3), 216–220, 1978.

Boyd, T. J. M., and J. J. Sanderson, *Plasma Dynamics*, Barnes and Noble, New York, 1969.

Feldman, W. C., J. R. Asbridge, S. J. Bame, M. D. Montgomery, and S. P. Gary, Solar wind electrons, *J. Geophys. Res.*, *80*, 4181–4196, 1975.

Feldman, W. C., S. J. Bame, S. P. Gary, J. T. Gosling, D. J. McComas, and M. F. Thomsen, Electron heating within the Earth's bow shock, *Phys. Rev. Lett.*, *49*, 199–201, 1982.

Feldman, W. C., R. C. Anderson, S. J. Bame, J. T. Gosling, R. D. Zwickl, and E. J. Smith, Electron velocity distributions near interplanetary shocks, *J. Geophys. Res.*, *88*, 9949–9958, 1983a.

Feldman, W. C., S. J. Bame, S. P. Gary, J. T. Gosling, D. J. McComas, M. F. Thomsen, G. Paschmann, and M. M. Hoppe, Electron velocity distributions near the Earth's bow shock, *J. Geophys. Res.*, *88*, 96–110, 1983b.

Forslund, D. W., and C. R. Shonk, Formation and structure of electrostatic collisionless shocks, *Phys. Rev. Lett.*, *25*, 1699–1702, 1970.

Goodrich, C. C., and J. D. Scudder, The adiabatic energy change of plasma electrons and the frame dependence of the cross-shock potential at collisionless magnetosonic shock waves, *J. Geophys. Res.*, *89*, 6654–6662, 1984.

Hull, A. J., Partition of temperature between electrons and ions across collisionless, fast mode shocks, Ph.D. thesis, Univ. of Iowa, Iowa City, 1998.

Hull, A. J., J. D. Scudder, L. A. Frank, W. R. Paterson, R. J. Fitzenreiter, C. T. Russell, S. Kokubun, and T. Yamamoto, Coherent electron heating and phase space signatures at strong shocks (abstract), *Eos Trans. AGU*, *78*(17), Spring Meet. Suppl., S281, 1997.

Hull, A. J., J. D. Scudder, L. A. Frank, W. R. Paterson, and M. G. Kivelson, Electron heating and phase space signatures at strong and weak quasi-perpendicular shocks, *J. Geophys. Res.*, *103*, 2041–2054, 1998.

Montgomery, M. D., J. R. Asbridge, and S. J. Bame, Vela 4 plasma observations near the Earth's bow shock, *J. Geophys. Res.*, *75*, 1217–1230, 1970.

Morse, R. L., Adiabatic time development of plasma sheaths, *Phys. Fluids*, *8*, 308–314, 1965.

Ogilvie, K. W., J. D. Scudder, and H. Doong, The electron spectrometer experiment on ISEE-1, *IEEE Trans. Geosci. Electron.*, *16*(3), 261–265, 1978.

Russell, C. T., The ISEE-1 and -2 fluxgate magnetometers, *IEEE Trans. Geosci. Electron.*, *16*(3), 239–242, 1978.

Schwartz, S. J., M. F. Thomsen, S. J. Bame, and J. T. Stansberry, Electron heating and the potential jump across fast mode shocks, *J. Geophys. Res.*, *93*, 12,923–12,931, 1988.

Scudder, J. D., The field aligned flow approximation for electrons within layers possessing a normal mass flux: A corollary to the deHoffmann-Teller theorem, *J. Geophys. Res.*, *92*, 13,447–13,455, 1987.

Scudder, J. D., A review of the physics of electron heating at collisionless shocks, *Adv. Space Res.*, *15*(8/9), 181–223, 1995.

Scudder, J. D., D. L. Lind, and K. W. Oligilvie, Electron observations in the solar wind and magnetosheath, *J. Geophys. Res.*, *78*, 6535–6548, 1973.

Scudder, J. D., E. C. Sittler Jr., and H. S. Bridge, A survey of the plasma electron environment of Jupiter: A view from voyager, *J. Geophys. Res.*, *86*, 8157–8179, 1981.

Scudder, J. D., A. Mangeney, C. Lacombe, C. C. Harvey, T. L. Aggson, R. Anderson, J. T. Gosling, G. Paschmann, and C. T. Russell, The resolved layer of a collisionless, high β, supercritical, quasi-perpendicular shock wave, 1, Rankine-Hugoniot geometry, currents, and stationarity, *J. Geophys. Res.*, *91*, 11,019–11,052, 1986a.

Scudder, J. D., A. Mangeney, C. Lacombe, C. C. Harvey, and T. L. Aggson, The resolved layer of a collisionless, high β, supercritical, quasi-perpendicular shock wave, 2, Dissipative fluid electrodynamics, *J. Geophys. Res.*, *91*, 11,053–11,073, 1986b.

Scudder, J. D., A. Mangeney, C. Lacombe, C. C. Harvey, C. Wu, and R. Anderson, The resolved layer of a collisionless, high β, supercritical, quasi-perpendicular shock wave, 3, Vlasov electrodynamics, *J. Geophys. Res.*, *91*, 11,074–11,097, 1986c.

Thomsen, M. F., J. T. Gosling, S. J. Bame, K. B. Quest, D. Winske, W. A. Livesey, and C. T. Russell, On the noncoplanarity of the magnetic field within a fast collisionless shock, *J. Geophys. Res.*, *92*, 2305–2314, 1987a.

Thomsen, M. F., M. M. Mellott, J. A. Stansberry, S. J. Bame, J. T. Gosling, and C. T. Russell, Strong electron heating at the Earth's bow shock, *J. Geophys. Res.*, *92*, 10,119–10,124, 1987b.

Viñas, A. F., and J. D. Scudder, Fast and optimal solution to the Rankine-Hugoniot problem, *J. Geophys. Res.*, *91*, 39–58, 1986.

Whipple, E. C., The signature of parallel electric fields, *J. Geophys. Res.*, *82*, 1525–1531, 1977.

Wygant, J. R., M. Bensadoun, and F. S. Mozer, Electric field measurements at subcritical, oblique bow shock crossings, *J. Geophys. Res.*, *92*, 11,109–11,121, 1987.

R. J. Fitzenreiter and K. W. Ogilvie, NASA Goddard Space Flight Center, Greenbelt, MD 20771.

A. J. Hull, Space Science Laboratory, University of California, Berkeley, CA 94720. (ahull@ssl.berkeley.edu)

J. A. Newbury and C. T. Russell, Institute of Geophysics and Planetary Physics, University of California, Los Angeles, CA 90095.

J. D. Scudder, Department of Physics and Astronomy, University of Iowa, Iowa City, IA 52242. (jds@hydra.physics.uiowa.edu)

(Received July 30, 1999; revised February 24, 2000; accepted March 2, 2000.)